

## Physicochemical and Mechanical Characterization of Ceramic Materials from Meknes Region (Morocco)

Hamza Mesrar<sup>1\*</sup>, Laila Mesrar<sup>2</sup>, Raouf Jabrane<sup>1</sup>

<sup>1</sup> ISGR, Laboratory of Intelligent Systems, Georesources and Renewable Energies, Geology Department, Faculty of Sciences and Technologies of Fez, Sidi Mohamed Ben Abdellah University, B.P. 2022, Fez, Morocco

<sup>2</sup> Department of Genie Civil, Laboratory LOMC UMR CNRS, University Havre, 53 Rue de Prony, 76600 Le Havre, France

\* Corresponding author's e-mail: hamza.mesrar@usmba.ac.ma

### ABSTRACT

This scientific paper presents a comprehensive study of the physical and chemical properties of a clay sample collected from Meknes region of Morocco. X-ray diffraction analysis revealed the presence of kaolinite, muscovite, and quartz minerals in the clay sample. X-ray fluorescence analysis showed that the sample contained a significant amount of aluminum and silica. The Atterberg limit test indicated that the clay has a high plasticity index and is classified as a clay of low to medium plasticity. The ATG\_DSC analysis revealed that the sample underwent multiple endothermic reactions, including dehydration, dehydroxylation, and decarbonation, at different temperature ranges. Shrinkage and weight loss experiments showed that the clay exhibited high shrinkage and weight loss upon drying. SEM-EDX analysis provided information on the microstructure and elemental composition of the clay sample. The water absorption test revealed that the clay has a low water absorption capacity. The three-point flexural test showed that the clay bricks had high flexural strength, which makes it suitable for use in high-stress applications. Overall, the results suggest that the clay sample can be used in a variety of applications, including building materials, ceramics, and other industrial uses.

**Keywords:** clay bricks, X-ray diffraction, flexural strength, mineralogy.

### INTRODUCTION

Clay bricks are an ancient knowledge that has been used for centuries in construction and their popularity remains high due to their durability, strength and versatility. These building bricks are made from a mixture of clay and water that is molded and then fired at high temperatures to create a hard, durable material that can withstand various weather conditions and other stresses. In this article, the properties of clay bricks, including their chemical, physical and mineralogical composition (Phonphuak et al., 2016), as well as their manufacturing process and applications in construction and masonry (Cultrone et al., 2004; Tsozué et al., 2017) were explored. The advantages and inconveniences of using clay bricks as a building material were also examined and tips for

choosing the best type of clay for a particular application were provided. The characteristics and performance of clay bricks must include several parameters like the study of certain geotechnical characteristics to obtain a reliable and quality building material for construction and masonry projects, namely grain size, Atterberg limits, firing ranges, shrinkage and weight loss when air dried or at different heating temperatures, water absorption tests, thermal conductivity and flexural strength (Srisuwan and Phonphuak 2020; Cruz et al., 2020; Labò and Marini 2022).

Clay minerals have a large range of solid solutions with a rearrangement of chemical elements to create other clay minerals called neoformation phenomenon, as well as a great capacity to form mixed crystals by interstratification (Reynolds 1980; Grim 1962). Our study area focuses on the

Mansory quarry which is located in the north-western part of Morocco, in the Meknes region, all along the outer limit of the South-Rifain chain in contact with the Sais basin. The external Prerif consists mainly of gravitational aquifers with a chaotic structure resulting from the destruction of the aquifer fronts by moving outwards and is composed of a marly-sandy matrix of the Upper Miocene (Lajat et al., 1975; Tejera et al., 1995; Maychou 2009; de Lamotte 1987).

In order to obtain a finished product with an acceptable quality in the construction industry and to reduce the energy needed for its production to protect the environment, clays must be studied deeply. Several researchers have studied the potential uses of marl materials for fired bricks (Mesrar et al., 2021), their mechanical characterization (Calderón et al., 2023; Xiong et al., 2023) and their utilization in lightweight aggregates (Mesrar et al., 2023), or as a reinforced geopolymer (Silva et al., 2020), other works focused on the valorization of fired bricks with wood and fly ash (Djenabou et al., 2023; Elavarasan et al., 2021), landfill leachates (Ibrahim et al., 2022), palm kernel shells (Sarani et al., 2023) or recycled industrial slag (Gencel et al., 2021). The purpose of this work was to have the strongest, volumetrically stable bricks without spending a lot of energy for their manufacture. Sampling was carried out in five regions north of Meknes. The Prerif consists mainly of gravitational aquifers with a chaotic structure resulting from the destruction of the aquifer fronts by moving outwards and is composed of a marly-sandy matrix of the Upper Miocene

## EXPERIMENTAL DETAILS

### Preparation of the clay brick samples

In this study, the marl used came from the al mansori quarry, Meknes, Morocco (Fig. 1). The marl specimens undergo oven drying at 105°C for 24 hours, then are cut into quarters to collect a representative specimen of the material, then manually ground to a reduced particle size and finely ground for 5 minutes in an agate mill. The bricks are elaborated from samples of marl with an addition of mixing water, so the paste was well kneaded for 15 minutes; then, a metal mold size (8 cm long, 4 cm wide and 1.5 cm thick) was used to obtain the bricks. The bricks were then weighed, marked with two diagonal segments (50 mm long) and finally dried to allow the measurement of shrinkage and weight loss at room temperature. Once stabilized, the bricks were dried in an oven at 105°C for 24 hours and the firing process was started in a muffle kiln for 1.5 hours, allowing measurements of firing shrinkage, weight loss, and bending strength at each temperature, including 900°C to 1100°C in increments of 100°C (Figure 2).

### Chemical analysis

#### X-ray diffraction (XRD) analysis

The chemical composition of the clays was determined using X-ray diffraction analysis with a Philips XPERT-PRO PW3064 diffractometer equipped with copper K $\alpha$  1.2 radiation. Fluorescence spectrometry was also employed using

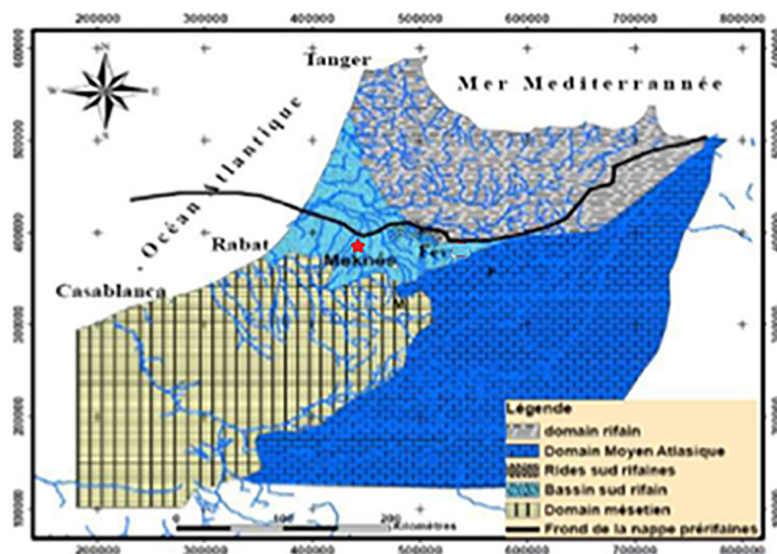
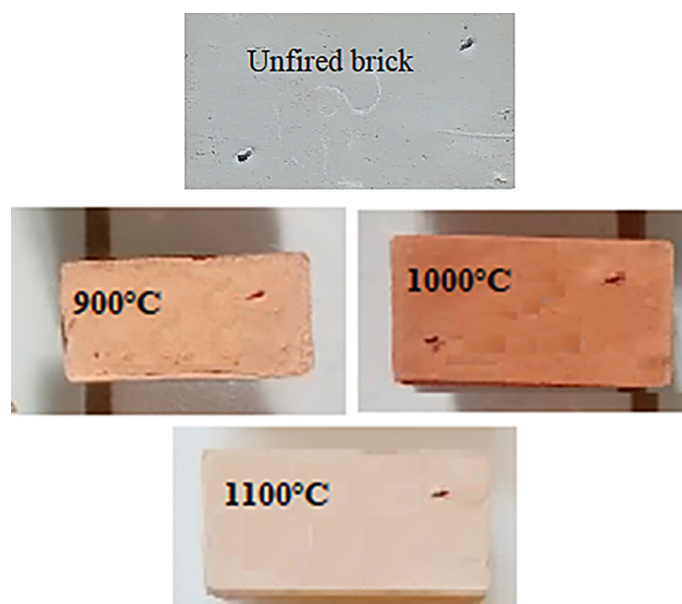


Fig. 1. Geological location of Meknes area, Morocco (Taltasse 1953, modified)



**Fig. 2.** Ceramic bricks manufactured from clay treated at different temperatures 900, 1000 and 1100 °C

pressed powder pellets and irradiation with a primary X-ray beam from an X-ray tube that produces the emission of fluorescent X-rays with discrete energies characteristic of the elements present in the sample. These analyses were conducted at the National Center for Scientific and Technological Research of Rabat (NCSTR) in Morocco.

### Physical analysis

#### TGA/DSC

The TGA/DSC 3+ simultaneous thermal analyzer utilizes a microbalance from a leading weighing technology company, providing reliable results. Its features include independent weighing of sample position, automatic calibration using built-in weights, a wide measuring range, and exceptional minimum weight performance and weighing accuracy. This instrument can analyze various sample types at high temperatures up to 1600 °C. Additionally, the integration of a DSC sensor allows for simultaneous measurement of thermal events, such as melting and crystallization, providing precise transition temperature data.

#### Bigot curve

The Bigot curve provides the information about the drying behavior of ceramic bricks, and shows the evolution of two characteristic phases of drying process: shrinkage according to weight loss and successive phase of stabilization.

#### Atterberg limits

The plastic and liquid Atterberg limits are two fundamental measurements of the crucial water concentrations of fine-grained soil. The test is conducted by using standard (NF P 94-051).

#### Water absorption

In this test, water absorption was evaluated by immersion using an international standard (NBN B 15-215(1989)). This test provides some insight into the porosity and, in turn, the material's resistance.

#### Mechanical analysis

The mechanical laboratory at FST Fez is where the bending strength tests were carried out (Figure 3). Using a maximum force of 50 KN and coupled to a computer system that runs software (EM 506), which gives the evolution of the bending resistance (N) according to the displacement (mm). Using the equation for three-point bending, the maximum resistance of flexural strength was determined:

$$R = \frac{3FL}{2b \cdot d^2} \quad (1)$$

The results are expressed in the mega Pascal (MPa). The flexural strength of fired bricks is evaluated.

#### Scanning electron microscope (SEM)

The SEM image is captured using a pressure-controlled instrument consisting of various

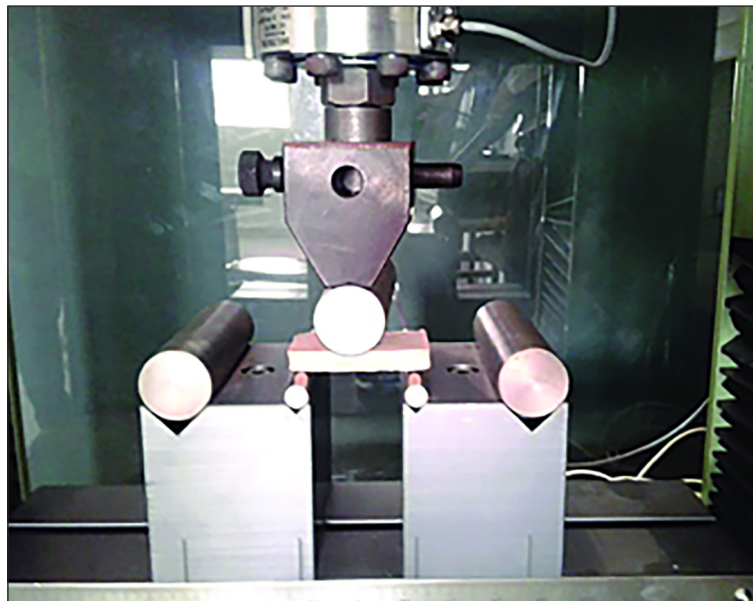


Fig. 3. Flexural strength test to check tension in bricks

components, including a cathode that generates the electron beam, a condenser system that produces a reduced image of the cross-over, an objective lens that projects the image onto the object, a scanning system comprising deflection coils to move the probe over the object, as well as a detector that detects signals from a fluorescent screen and produces a black and white image.

## RESULTS AND DISCUSSION

### Mineralogical and chemical characterization

Depending on the geological environment or kind of rocks in the location where the geographic

clays are produced from and the extent of weathering, geographic clay samples show different mineralogical composition (Mesrar et al., 2023; Mesrar et al., 2020). X-ray diffraction was carried out on raw marl in the Meknes region of Morocco to study reflections at the base of individual clay minerals and impurities. Figure 4 displays the X-ray diffraction (XRD) patterns of the marl powder sample without heat treatment. Moreover, the Rietveld method, implemented in the HighScore Plus software, is a powerful tool for analyzing X-ray powder diffraction data of materials like marl. This method is based on the principle of least squares refinement, where the crystal structure and the background are simultaneously refined to obtain the best fit between the observed

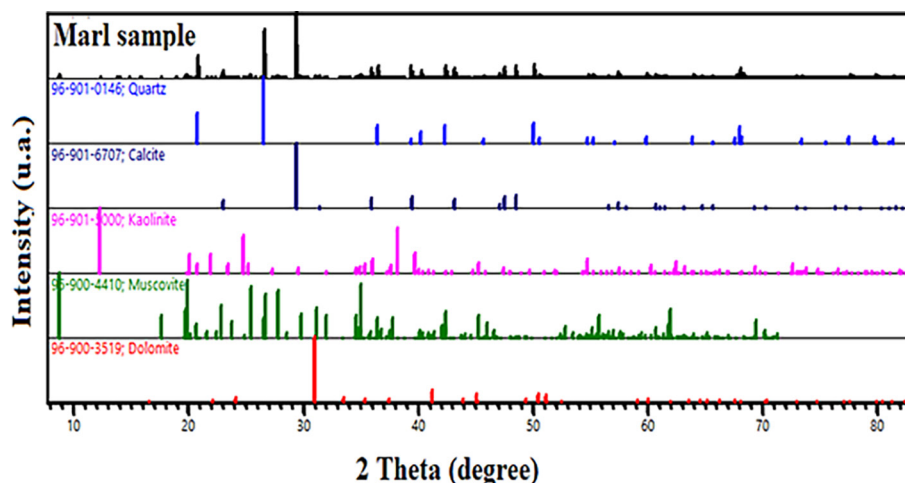


Fig. 4. X-ray powder diffraction analysis of marl

and calculated diffraction patterns. By refining the crystal structures of each phase and the background simultaneously, the Rietveld method can provide accurate and precise information about the composition, crystallinity, and microstructure of the material. The given sample of marl reveals that it primarily consists of muscovite (36%) (Figure 5), followed by calcite (18%), quartz (21%), kaolinite (10%), and dolomite (15%). The high percentage of muscovite suggests that the marl may have formed in a sedimentary environment with high amounts of mica-rich minerals.

The presence of calcite indicates the possibility of the marl being a sedimentary rock formed from the accumulation of calcareous materials. Similarly, the presence of quartz points towards a sedimentary origin in a high-energy environment. The small amounts of kaolinite and dolomite suggest secondary mineralization or alteration processes affecting the primary minerals in the marl. Overall, the mineralogical and chemical characterization of the marl provides a valuable insight into its geological history and potential applications.

The firing process at different temperatures (900, 1000 and 1100°C) enabled to identify the mineralogical alterations and changes these materials underwent as well as the discovery of new mineral phases. Moreover, the samples undergoing heat treatment can suffer changes in their physical properties. The X-ray diffraction patterns of the sample, processed at different temperatures from 900 to 1100°C, used in this analysis are presented in Figure 6. At 900°C, the presence of quartz (55%) (Figure 7), albite (28%), and gehlenite (17%) is observed. At 1000°C, illite and diopside appear with percentages of 5% and 65%, respectively. At 1100°C, illite and gehlenite are present with percentages of 10% and 18%, respectively, while quartz remains unchanged at all firing temperatures. As the temperature increases, the crystal structure of the minerals changes. Phyllosilicates and calcite are unstable at high temperatures and decompose into more stable minerals such as albite and gehlenite. However, albite is also unstable at higher temperatures, leading to the appearance of illite and diopside at 1000°C. The reappearance of illite and gehlenite at 1100°C is due to the reformation of minerals from the decomposition of albite and gehlenite at the previous temperature.

The reason for these transformations is due to the fact that minerals are composed of different

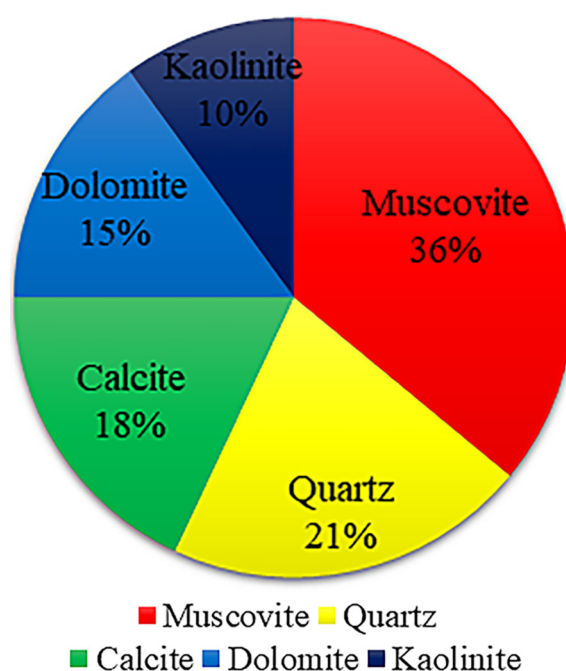


Fig. 5. Mineralogical composition of marl as illustrated by pie chart percentages

elements arranged in specific crystal structures. The temperature range of 20 to 600°C is associated with the loss of free and molecular water in clay minerals (Gencel et al., 2020). Kaolinite disappears at around 650°C (ELOuazzani et al., 2012), while the temperature range of 550 to 800°C corresponds to the decarbonation of calcite and dolomite, releasing CaO and periclase (Klaarenbeek 1961; Kreimeyer 1987). Firing up to 700°C does not cause significant mineralogical or textural transformations in clays. Quartz  $\alpha$  transforms into quartz  $\beta$  between 550 and 800°C, and at temperatures above 800°C, clay minerals disappear to form neoformal minerals like gehlenite (Jordán et al., 1999). Heat treatment (550–900°C) leads to dehydroxylation of clay minerals, resulting in the formation of aluminosilicate phases with kaolin having the highest pozzolanic activity (Strazzera et al., 1997).

Complete decomposition of dehydroxylated occurs at 950°C (Peters et al., 1978). At 1000°C, iron is trapped in the structure of calcium silicates and aluminosilicates (Castellanos et al., 2012). The presence of neoformal minerals, such as Illite, diopside, and gehlenite is observed at 1100°C, followed by vitrification, which becomes significant at high temperatures (Garzón et al., 2022). The results showed that the mineral composition of the sample changed as the temperature increased, with the appearance and disappearance of different minerals.

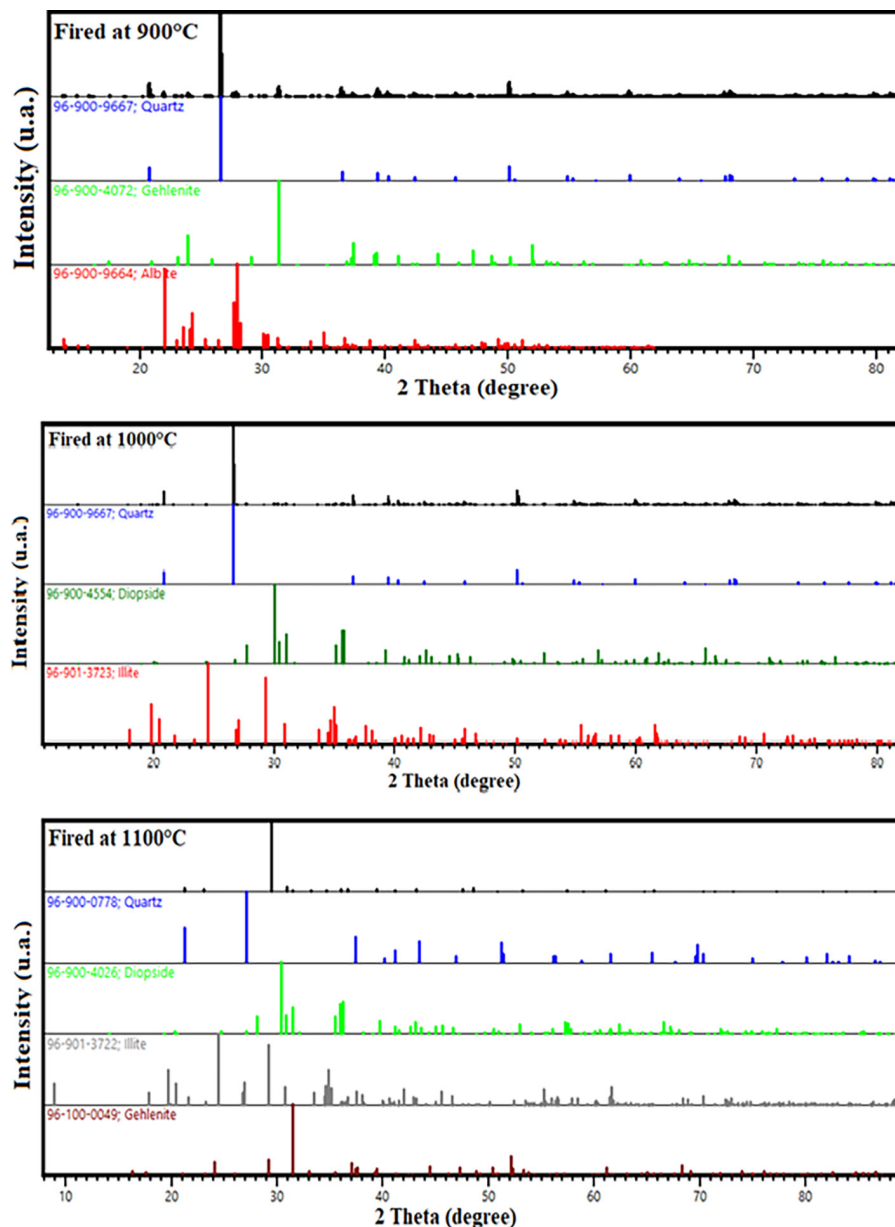


Fig. 6. X-ray powder diffraction analysis of marl firing at 900, 1000, and 1100°C

## Microstructure

The SEM images corresponding to the various types of soils investigated are displayed in Figure 8. SEM and EDX analyses were performed to examine the morphology, microstructure, and elemental composition of the clays before and after firing process. The electron microscopy analysis showed the occurrence of phyllosilicates arranged in sheets, as well as calcite and dolomite grains. Elemental maps of Si, Ca and Mg containing mineral phases show that the majority of the grains are quartz. The presence of calcium-rich grains could be attributed to the plagioclase content of the raw materials. However, it should be noted that gehlenite mineral is

formed during the sintering process and is among the Ca-containing phases. The results showed that calcite and dolomite crystals were present in the unfired material, correlating with decreasing levels of carbon and oxygen, as well as increasing levels of calcium and magnesium. This suggests that decarbonation of  $\text{CaCO}_3$  and  $\text{MgCO}_3$  occurred, leaving behind CaO (calcium oxide) and MgO (periclase) with  $\text{CO}_2$  degassing. These decarbonation and burnt organic matter led to an increase in porosity. With increasing temperature, the particles fused together and gave rise to new, fine-grained crystals in the matrix. The low degree of vitrification observed is attributed to the presence of carbonate oxide, which is a characteristic of marl materials.

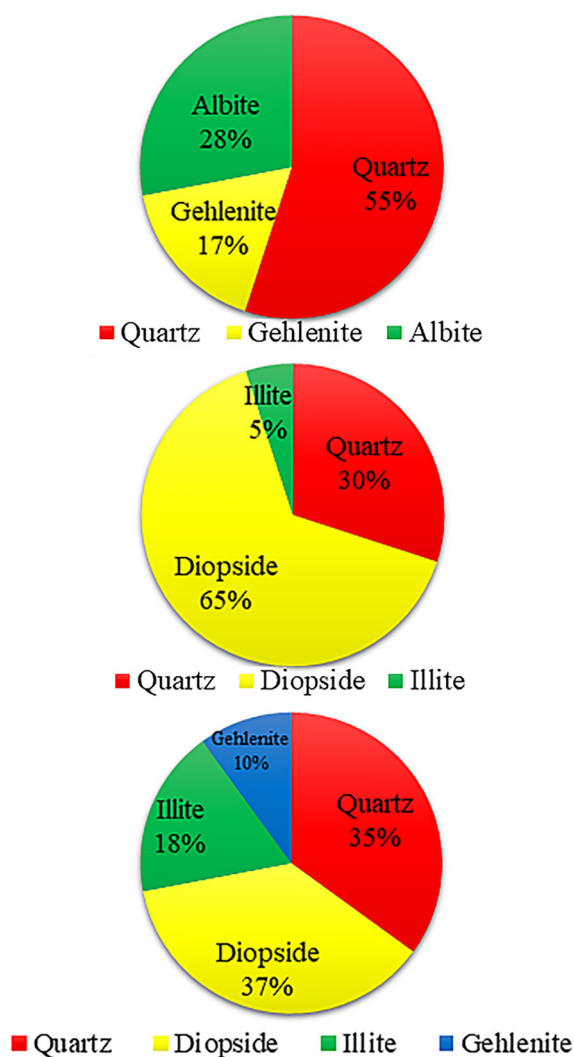


Fig. 7. Mineralogical composition of marl firing at 900, 1000, and 1100°C as illustrated by pie chart percentages

### X-ray fluorescence

Table 1 gives the chemical composition of the samples. It appears that silica, alumina and calcium are the dominant elements in the samples ( $\pm 70\%$ ). The iron oxide ( $\text{Fe}_2\text{O}_3$ ) is affected by firing, which causes color and texture variations in the heated clays. The color caused by iron oxide is related to the ratio of the amounts of  $\text{Fe}_2\text{O}_3$  and CaO elements in the sample material (L. Mesrar et al., 2021; Dondi 1999). In the marl samples, carbonates are present at relatively higher content ( $>13.7\%$ ), indicating the presence of calcite and dolomite, the refractory minerals that can also contribute to the fusion (Zhang et al., 2013).

Low concentrations of clay minerals are related the low rate of alkaline oxides ( $\text{K}_2\text{O}$ ,  $\text{Na}_2\text{O}$ ) ( $\approx 2\%$ ) (Dubois et al., 2011; Achour et al., 2014).

Their concentration is within the limits allowed for clay designed for the brick industry. (Strazzera et al., 1997) In addition, the loss on ignition is very high (39%). This is assigned to the release of adsorbed and crystalline water, decomposition of carbonates, oxidation of sulfides, and combustion of organic matter. On the basis of these results, the samples of marls used in this study have acceptable properties with low refractory properties.

### Geotechnical and ceramic tests

#### ATG-DSC

ATG-DSC (thermogravimetry – differential scanning calorimetry) is a thermal analysis technique used to study the thermal properties of materials. It involves measuring the changes in weight and heat flow of a sample as it is subjected to a controlled temperature program. ATG-DSC can provide the valuable information about the thermal stability, phase transitions, and decomposition of a material. By measuring the temperature at which a sample loses or gains weight, it is possible to determine the thermal stability of the material. The heat flow measurements obtained from DSC can provide the information about the enthalpy changes associated with phase transitions, such as melting or crystallization, and can also detect the presence of impurities or additives in the material.

A significant decrease in mass and heat flow up to 760°C which reaches 18% can be observed, mainly due to the loss of water and the decomposition of carbonates. From 770°C to 1100°C, it is noticed that the weight loss becomes low and the heat flow increase (Figure 9). This information is important for understanding the thermal behavior of the sample and its constituent minerals, and can aid in the interpretation of other thermal analysis data such as DSC.

The thermogram got by differential scanning calorimetry of raw clay at a heating rate of 20°C/min in a temperature range of 20 to 1100°C (Figure 9) reports three endothermic transformation:

- Dehydration (105–180°C), which corresponds to the removal of free and molecular water;
- The dehydroxylation may involve three chemical reactions between 420 and 600°C. The first reaction is related to the decomposition of kaolinite into metakaolin and involves a structural change from octahedral to tetrahedral aluminum, which results a loss of crystallinity. The second reaction takes place at

573°C and involves the transformation from  $\alpha$ -quartz, which is a polymorph stable at 573°C, to  $\beta$ -quartz, which remains stable until 900–1000°C. The third reaction corresponds to the transformation of illite to dehydrated illite, with the layered structure of the initial illite remaining unaltered until 1100°C.

- Decarbonation has an endothermic peak at 842°C that occurs between 700 and 900°C, where calcite ( $\text{CaCO}_3$ ) and dolomite ( $\text{MgCO}_3$ ) are decomposed into calcium oxide and periclase with  $\text{CO}_2$  emissions. It should be mentioned that the heating rate plays an important role in the evolution of the decomposition temperature.

### Atterberg limits

One of the most crucial parameters in the production of clayey material and shrinkage resulting from water loss from the prepared material to the finished burnt brick is plasticity (Mesrar et al., 2021). Atterberg limit results demonstrate that the samples have average plasticity index values of 26% (Table 2). The plasticity index provides an understanding of the soil through a value indicating the extent to which clay particles are present in a material and one of the crucial factors affecting the production of bricks (Boussen et al., 2016). Many variables influence soil plasticity, including geological formation, particle size

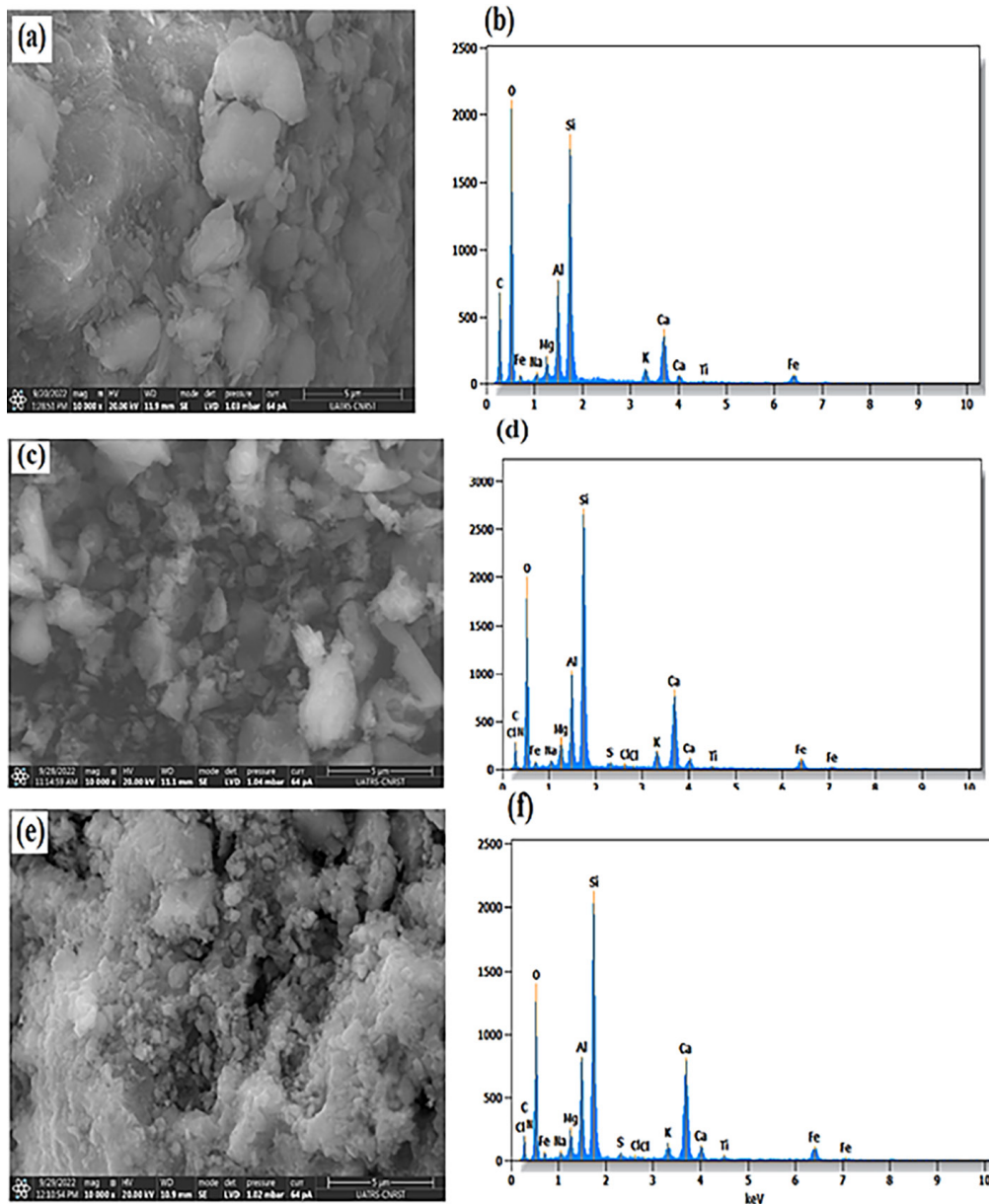


Fig. 8. SEM image and EDX typical of the marl

and distribution, mineral composition, impurities and organic matter (Nagaraj et al., 2014; Semiz 2017). Through evaluating the results of Atterberg limits tests, the samples plasticity is moderate and shows very close values. The graph shows that the sample has the moderate plasticity index, which is mainly due to the presence of clay minerals such as kaolinite and muscovite (Bautista-Marín et al., 2021). In this case, the sample is effective for the industry since it requires lesser shrinkage (Figure 10).

### Bigot curve

The Bigot curve gives the information about the air-drying of our bricks (Figure 11); this test shows the evolution of two characteristic phases of the drying process: shrinkage as a function of weight loss and the successive stabilization phases (Boussen et al., 2016). The control of the drying parameters offers many options to determine the optimal drying time and energy consumption (Madlener et al., 2007). It was found that the obtained bricks are homogeneous and present acceptable results. Sample presents an acceptable shrinkage. This result confirms Atterberg limit. The complete stabilization of the shrinkage and weight loss is observed on the 5th day.

### Firing bricks

The author in the literature (Dondi 1999; González and Ruiz 2006; Hajjaji et al., 2010;

Jordan et al., 2008) provides a thorough account of the phase transitions that take place during the thermal treatment of calcareous clays.

The sintering process is influenced by phase changes related to hydration, hydroxylation, carbonate decomposition and the firing step. Fired clay bodies shrink and lose weight as a result of these transformations. For dimensional management of finished ceramic products, linear shrinkage is a crucial indicator of material porosity. The results for linear firing shrinkage, weight loss, and water absorption of burned bricks are presented in Figures 12 and 13, respectively. Clay minerals

**Table 1.** Chemical compositions from X-ray fluorescence (in wt.%) compared with natural clay used for brick production in France (Kornmann 2009), (a) maximum value, (b) minimum value

Sample	Clay	a	b
SiO <sub>2</sub>	42.34	35	80
Al <sub>2</sub> O <sub>3</sub>	15.25	8	30
CaO	13.74	2	10
Fe <sub>2</sub> O <sub>3</sub>	3.52	0	1.5
MgO	3.11	0.5	18
K <sub>2</sub> O	1.84	0	5
TiO <sub>2</sub>	0.67	0.1	1.5
Na <sub>2</sub> O	0.65	0.1	4.5
P <sub>2</sub> O <sub>5</sub>	0.21	0	1.5
Cl	0.12	0	1
Other oxides	0.12	-	-
LOI		3	18

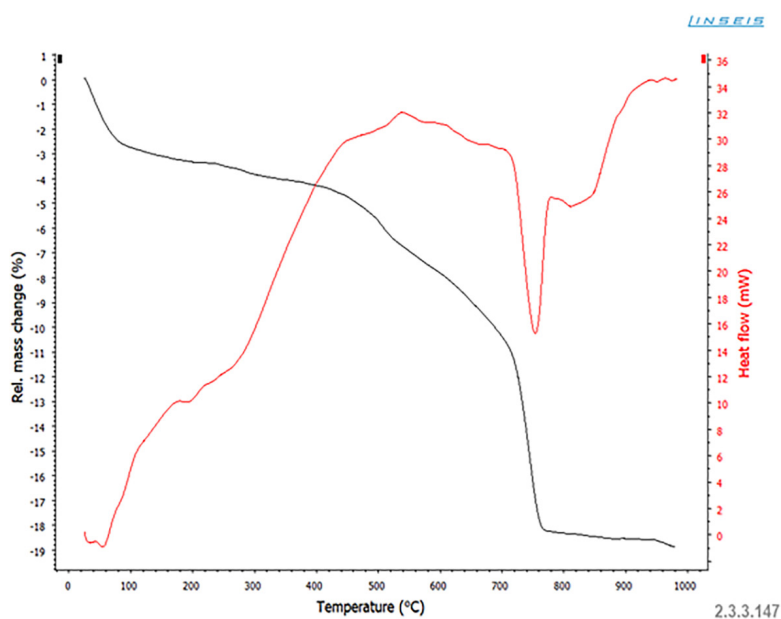


**Fig. 9.** ATG-DSC analysis of the marl

are used in brick making to stabilize suspensions (in the wet route), provide plasticity for shaping, and provide mechanical strength for burnt bodies. The clay serves as a flux (such as muscovite) or as a precursor (such as kaolinite) during firing. Carbonates, which are fine-grained, generate pores during firing and sintering by surface diffusion; flux, which forms a liquid phase at high

temperatures and aids in densifying the ceramic body by a viscous flow (Dondi et al., 2014).

Above 900°C, all bricks show minor linear shrinkage (0.70 to 2.15%). Through the dissolution of carbonates (calcite) and the loss of inter-layer water in phyllosilicates, clay formations degrade at these temperatures. The linear shrinkage varies from 2.15% at 1000°C. By acting as a neutral phase within the transformed clay phases, the carbonates perform the part of melting. The dehydroxylated silicate molecules are thus in an unstable state, known as the metaphase, and then made up of meta-clays because they have lost their original crystalline property. The porosity is directly proportional to the water absorption

**Table 2.** Atterberg’s limits

Atterberg’s limits	Raw material
Plastic limits, PL (%)	23.05 -+ 5
Liquid limits, LL (%)	49.2 -+ 5
Plastic index, PI (%)	26.14 -+ 5

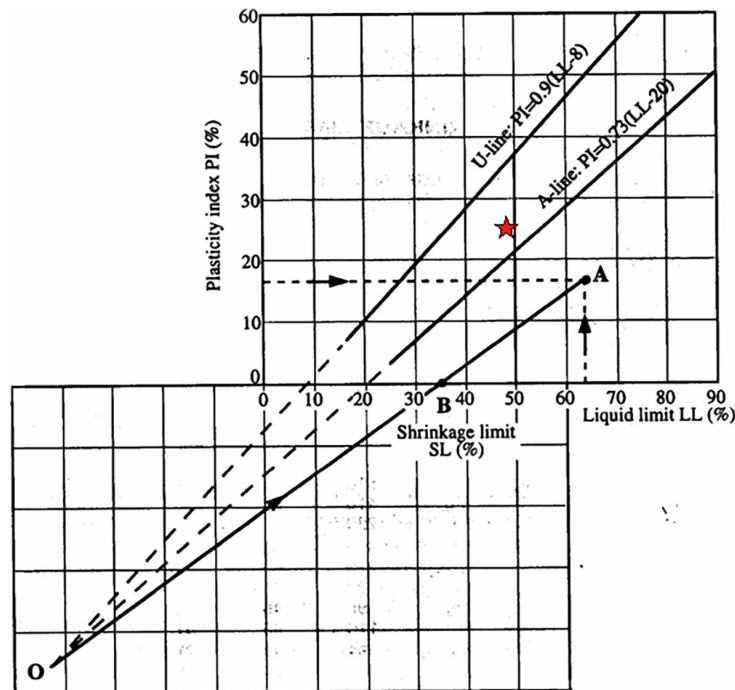


**Fig. 10.** Relation sheep of plasticity index and liquidity limit from shrinkage limit (Snethen et al., 1977)

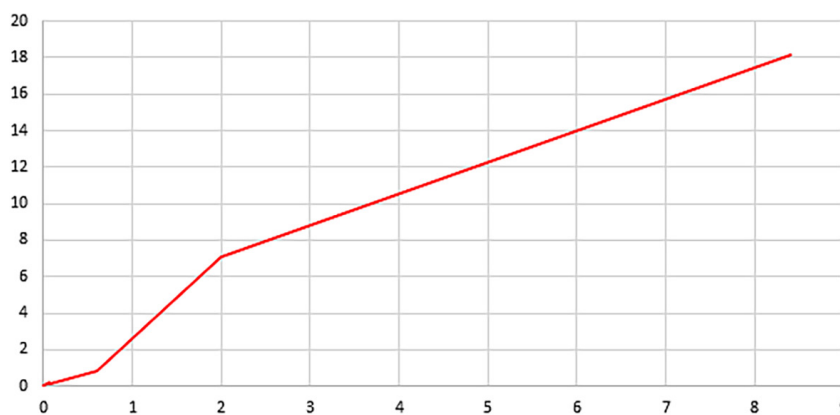


**Fig. 11.** Bigot’s curve of bricks

which is an important value when talking about external structural elements of buildings such as paving stones and for internal use this value is not fixed according to the code EN 771-1 (Gencil et al., 2020). Water absorption rate refers to the rate at which a material absorbs water when it is in contact with it. This percentage can depend on a variety of factors, including its porosity, surface area, and chemical composition of material (Raimondo et al., 2009).

The bricks that have a high water absorption rate (13.5%) are those that have been fired at a temperature of 1000°C and fall within the scope of IS 3495-2. According to this standard, the maximum allowable water absorption rate by weight for such bricks should not exceed 15%. In contrast, at 1100°C, this rate reduces and reaches 12%. Flexural strength refers to a material’s ability to resist bending or deformation when subjected to an applied force. In the case of bricks, flexural strength is an important property that affects their performance in applications such as construction and masonry. The flexural strength of bricks is typically measured using a testing method called the three-point bending test, which involves applying a load to a brick supported at two points and

measuring the amount of force required to cause it to bend or break. The results of this test can be used to determine the suitability of a particular type of brick for a given application, as well as to compare the performance of different types of bricks under similar conditions.

The densification of bricks results from a number of physical and chemical reactions, including dehydration of hydroxide, dehydroxylation of clay minerals, phase transformations and partial melting that generate a glassy phase (Milheiro et al., 2005). By diffusion and surface flow, carbonate decomposition creates pores in the bricks during firing and sintering. This liquid phase is created at high temperature and densifies the brick pieces by viscous flow (Dondi et al., 2014). The other author, who employs a hydraulic press, can achieve a higher final product resistance. However, even though making bricks using a simple molding technique is an ancient method, the materials obtained in this study are of high quality. As a result, with the basic methods employed, all the results of the mechanical tests, as depicted in Figure 4, surpass the standard for building materials, ASTM-C674 (1999), which requires a minimum of  $\geq 2.5$  Mpa (Benahsina et

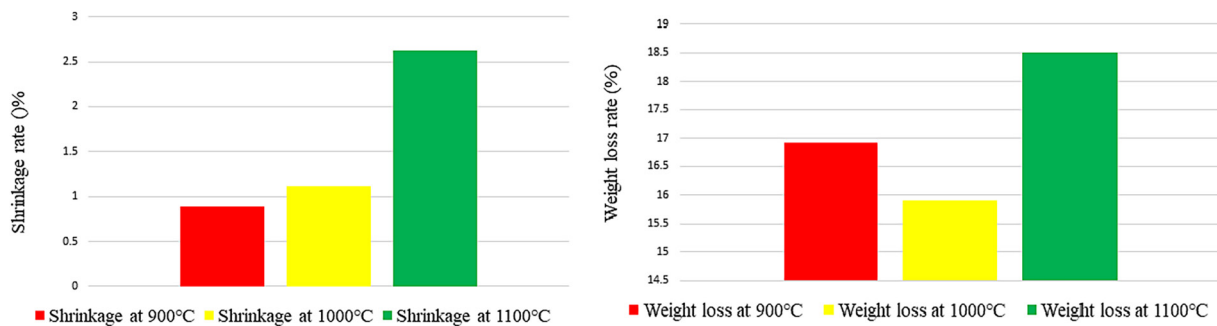


Fig. 12. Shrinkage and weight loss of sample

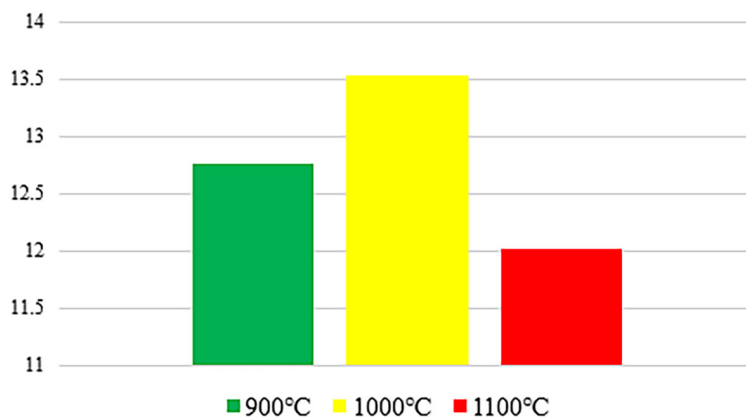


Fig. 13. Percentage of water absorption in wt. %

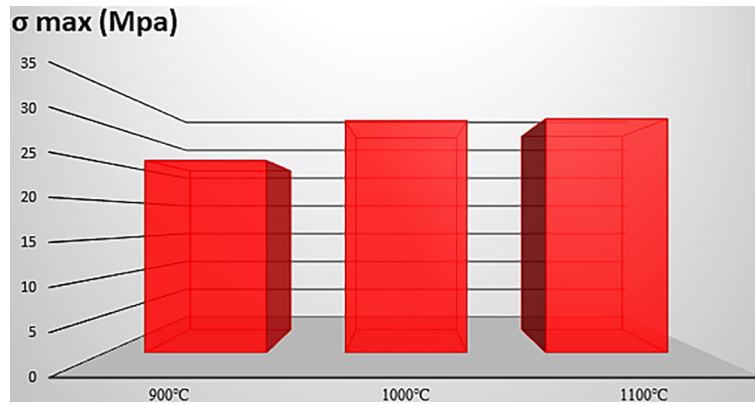


Fig. 14. Results of three-point flexural strength testing on the fired bricks at different temperatures

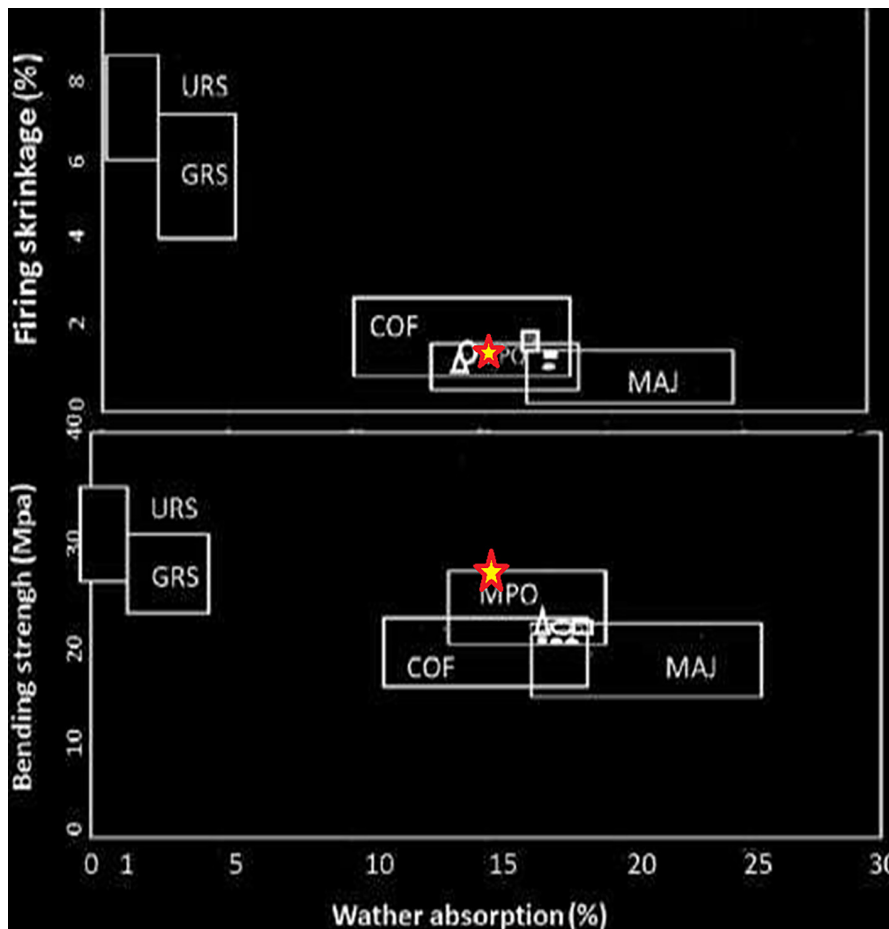


Fig. 15. Classification of tested materials in the reference industrial diagram from(Dondi et al., 2001). MAJ majolica, COF cottoforte, MPO monoporosa, GRS glazed red stoneware, URS unglazed red stoneware

al., 2022). When these crystalline structures exceed their stability limits, they partially decompose in the ceramic process, allowing other minerals to form. It is well known that heterogeneous clays have a complex mineralogical composition, which complicates the investigation of new mineralization, and the disappearance of mineral phases present in the raw material (Dondi et al.,

2001). It is noticeable in Figure 14, that the mechanical strength increases proportionally with the increase of the firing temperature and reaches 30.8 MPa at 1000°C. Nonetheless, new minerals detected at this temperature (Figure 6 and 7) with random-oriented and pore-forming effects are most likely the reason for the compressive strength decrease to 30.8 MPa. These findings

suggest that these raw materials can be used to make ceramics, bricks, and tiles, because they have similar properties to other clays used in the industry in North Africa and elsewhere (Hachani et al., 2012; Dondi 1999; El Ouahabi et al. 2014; Dondi et al., 2021).

### Classification on an industrial reference chart

Dondi published a categorization diagram that considered water absorption, firing shrinkage, and bending strength (Dondi et al., 2001). This classification was utilized for these marls, and two maximum temperatures were considered: 1000°C for the traditional cycle, which corresponds to “cottoforte,” and 1100°C for the rapid cycle, which corresponds to “monoporosa.” It should be observed that the values of water absorption, linear shrinkage, and bending strength are always interdependent; hence, the lower the water absorption, the lower the linear shrinkage, and the greater the bending strength (Figure 15).

The findings from the tests appear in the diagram, and the fire behavior of the tested materials is compared to the technological requirements for ceramic tiles with colored bodies. The results show that the properties of the samples are appropriate in the body formulation for wall tiles, particularly in the case of monoporosa technology.

### CONCLUSIONS

In conclusion, the various analytical techniques used in this study have provided valuable insights into the physical and chemical properties of the material under investigation. The mineralogical composition of the material was revealed through X-ray and X-ray fluorescence analyses, which indicated the presence of minerals such as quartz, phyllosilicates like kaolinite, muscovite as well as carbonates such as calcite, and dominant elements such as silica, alumina, and calcium. The results of the Atterberg limit tests suggest that the samples exhibit low plasticity rank (>26.1) and low liquidity (>49.2) due to such factors as particle size and distribution, mineral composition, impurities, and organic matter content present in the marls. The ATG-DSC as well as shrinkage and weight loss tests yielded valuable information on the material’s thermal stability and behavior during heating, which can be highly beneficial for the fired brick industry. The SEM-EDX analysis

revealed the presence of phyllosilicates, calcite, and dolomite crystals in the unfired material. The levels of carbon and oxygen decreased, while the levels of calcium and magnesium increased along with temperature, indicating a correlation between mineral content and temperature. The observed presence of phyllosilicate, calcite crystals in the unfired material through SEM-EDX analysis, suggests that  $\text{CaCO}_3$  underwent decarbonation during heating, leading to the formation of CaO (calcium oxide), and the release of  $\text{CO}_2$ . This decarbonation process, along with the burning of organic matter, resulted in increased porosity. The results of the water absorption test indicate that the material has a porosity and water retention capacity of less than 14%, meeting the requirements of the ASTM-C373 industry standard (1999). Finally, the results of the three-point flexural test demonstrate a direct correlation between the firing temperature and the material’s mechanical strength, which reaches 30.8 MPa at temperatures of 1000 and 1100°C. Overall, the combination of these techniques has provided a comprehensive understanding of the material’s properties, which will be valuable for its potential application in various fields such as construction industry.

### REFERENCES

1. Phonphuak N., Kanyakam S., Chindaprasirt P. 2016. Use of glass waste to improve the physical-mechanical properties of the clay brick. *Journal of Cleaner production*, 112, 3057–3062.
2. Cultrone G., Sebastián E., Elert K., De la Torre M.J., Cazalla O., Rodriguez N.C. 2004. Influence of mineralogy and firing temperature on brick porosity. *Journal of the European Ceramic Society*, 24(3), 547–564.
3. Tsozúé D., Nzeugang A.N., Mache J.R., Loweh S., Fagel N. 2017. Mineralogical, physico-chemical and technological characterization of clays from Maroua (Far-North, Cameroon) for use in ceramic bricks production. *Journal of Building Engineering*, 11, 17–24.
4. Srisuwan A., Phonphuak N. 2020. Physical property and compressive strength of fired clay bricks incorporated with paper waste. *Journal of Metals, Materials and Minerals*, 30(1).
5. Cruz P.J., Camões A., Figueiredo B., Ribeiro M.J., Renault J. 2020. Additive manufacturing effect on the mechanical behaviour of architectural stoneware bricks. *Construction and Building Materials*, 238, 117690.
6. Labò S., Marini A. 2022. In-plane flexural behavior of hollow brick masonry walls with horizontal

- holes. *Engineering Structures*, 273, 115086.
7. Reynolds R.C. 1980. Interstratified clay minerals
  8. Grim R.E. 1953. Clay mineralogy, 76(4), 317, LWW.
  9. Lajat D., Biju-Duval B., Gonnard R., Letouzey J., Winnock E. 1975. Atlantic extension of the outer part of the Betic-Ribbarian Arc. *Bulletin de la Societe geologique de France*, 7(4), 481–485.
  10. Tejera J., Boutakiout M., Ammar A., Ait Brahim L., El Hatimi N. 1995. The Central Rif Basins (Morocco); markers of out-of-sequence thrusting of terminal Miocene age in the core of the chain. *The Bulletin of the Geological Society of France*, 166(6), 751–761.
  11. Maychou S. 2009. Morphostructural study and GIS mapping of the Septentrional Rharb and Préfif (Morocco): seismotectonic analysis and deformation modeling of the Moulay Bousselham region (Doctoral dissertation, Bordeaux 1).
  12. De Lamotte D.F. 1987. The structure of the outer rift (Morocco): an update on the role of thrusting and gravity slides. *Journal of African Earth Sciences* (1983), 6(5), 755–766.
  13. Mesrar L., Benamar A., Mesrar H., Jabrane R. 2021. Physical and Mechanical Properties Improvement of Miocene Marls (Morocco) Doped by Iron Oxide  $Fe_2O_3$ . In: *Sustainable Environment and Infrastructure*. Springer, Cham, 259–269.
  14. Calderón S., Sandoval C., Araya-Letelier G., Aguilar V. 2023. A detailed experimental mechanical characterization of multi-perforated clay brick masonry. *Journal of Building Engineering*, 63, 105505.
  15. Xiong W., Zhu H., Xu J., Ma J., Luo C. 2023. Experimental investigation on physical and mechanical properties of excavated soil-and fine recycled concrete aggregate-based unfired clay bricks containing compound additives. *Case Studies in Construction Materials*, 18, e02057.
  16. Mesrar H., Mesrar L., Touache A., Jabrane, R. 2023. Manufacture of Clay Aggregate Doped with Pozzolan Destined for Lightweight Concrete. *Journal of Ecological Engineering*, 24(1), 349–359.
  17. Silva G., Kim S., Bertolotti B., Nakamatsu J., Aguilar R. 2020. Optimization of a reinforced geopolymer composite using natural fibers and construction wastes. *Construction and Building Materials*, 258, 119697.
  18. Djenabou S., Ndjigui P.D., Bukalo N., Ekosse G.I. 2023. Effect of the incorporation of Neem (*Azadirachta indica*) wood ash in Kodeck ceramic materials for the manufacture of fired bricks (Far-North Cameroon). *Heliyon*, 9(3).
  19. Elavarasan S., Priya A.K., Kumar V.K. 2021. Manufacturing fired clay brick using fly ash and M-Sand. *Materials Today: Proceedings*, 37, 872–876.
  20. Ibrahim A.K., Ismail G.A., Badr M.A., Badr, M.M. 2022. Incorporating of landfill leachate in fired-clay bricks manufacturing: An experimental study. *Process Safety and Environmental Protection*, 166, 558–564.
  21. Sarani N.A., Kadir A.A., Din M.F.M., Hashim A.A., Hassan M.I.H., Hamid N.J.A., Johan S.F.S. 2023. Physical-mechanical properties and thermogravimetric analysis of fired clay brick incorporating palm kernel shell for alternative raw materials. *Construction and Building Materials*, 376, 131032.
  22. Gencil O., Munir M.J., Kazmi S.M.S., Sutcu M., Erdogmus E., Velasco P.M., Quesada D.E. 2021. Recycling industrial slags in production of fired clay bricks for sustainable manufacturing. *Ceramics International*, 47(21), 30425–30438.
  23. Taltasse P. 1953. Geological and hydrogeological research in the Fez-Moknes lake basin, &c.
  24. Gencil O., Erdugmus E., Sutcu M., Ore O. H. 2020. Effects of concrete waste on characteristics of structural fired clay bricks. *Construction and Building Materials*, 255, 119362.
  25. El Ouazzani D.C., Bouamrane A., Mansouri K., Fokam C.B. 2012. Valorization of paper mill sludge in construction: mineralogical analysis of the impact of incineration conditions. *Journal of Materials and Environmental Science*, 3(4).
  26. Klaarenbeek F.W. 1961. The development of yellow colours in calcareous bricks, *Transactions of the British Ceramic Society*, 60, 738–772.
  27. Kreimeyer R. 1987. Some notes on the firing colour of clay bricks, *Applied Clay Science*, 2 175–183.
  28. Jordán M.M., Boix A., Sanfeliu T., De la Fuente C. 1999. Firing transformations of cretaceous clays used in the manufacturing of ceramic tiles. *Applied Clay Science*, 14(4), 225–234.
  29. Strazzera B., Dondi M., Marsigli M. 1997. Composition and ceramic properties of tertiary clays from southern Sardinia (Italy). *Applied Clay Science*, 12(3), 247–266.
  30. Peters T., Iberg R., Mumenthaler T. 1978. Comparative study of the use of a quartz poor sand and a pure quartz sand for lime silica bricks and the kinetics of the hydrothermal hardening mechanism. *Cement and Concrete Research*, 8(4), 415–424.
  31. Castellanos A.O.M., Ríos R.C.A., Ramos G.M.A., Plaza P.E.V. 2012. A comparative study of mineralogical transformations in fired clays from the Laboyos Valley, Upper Magdalena Basin (Colombia). *Boletín de Geología*, 34(1), 43–55.
  32. Garzón E., Pérez-Villarejo L., Eliche-Quesada D., Martínez-Martínez S., Sanchez-Soto P.J. 2022. Vitrification rate and estimation of the optimum firing conditions of ceramic materials from raw clays: A review. *Ceramics International*.
  33. Dondi M. 1999. Clay materials for ceramic tiles from the Sassuolo District (Northern Apennines, Italy).

- Geology, composition and technological properties. *Applied Clay Science*, 15(3–4), 337–366.
34. Zhang Q., Liu H., Qian Y., Xu M., Li W., Xu J. 2013. The influence of phosphorus on ash fusion temperature of sludge and coal. *Fuel processing technology*, 110, 218–226.
  35. Kornmann M. 2009. Clay materials: Basic materials and fabrication. *Engineering Techniques. Construction*, (C905v2).
  36. Dubois V., Zentar R., Abriak N.-E., Grégoire P. 2011. Fine sediments as a granular source for civil engineering, *European Journal Environnement Civil Engineering*, 15, 137–166.
  37. Achour R., Abriak N.E., Zentar R., Rivard P., Gregoire P. 2014. Valorization of Unauthorized Sea Disposal Dredged Sediments as a Road Foundation Material. *Environmental Technology*, 35(16), 1997–2007.
  38. Boussen S., Sghaier D., Chaabani F., Jamoussi B., Bennour A. 2016. Characteristics and industrial application of the Lower Cretaceous clay deposits (Bouhedma Formation), Southeast Tunisia: Potential use for the manufacturing of ceramic tiles and bricks. *Applied Clay Science*, 123, 210–221.
  39. Nagaraj H.B., Sravan M.V., Arun T.G., Jagadish K.S. 2014. Role of lime with cement in long-term strength of Compressed Stabilized Earth Blocks. *International Journal of Sustainable Built Environment*, 3(1), 54–61.
  40. Semiz B. 2017. Characteristics of clay-rich raw materials for ceramic applications in Denizli region (Western Anatolia). *Applied Clay Science*, 137, 83–93.
  41. Bautista-Marín J.D., Esguerra-Arce A., Esguerra-Arce J. 2021. Use of an industrial solid waste as a pigment in clay bricks and its effects on the mechanical properties. *Construction and Building Materials*, 306, 124848.
  42. Snethen D.R., Johnson L.D., Patrick D.M. 1977. An evaluation of expedient methodology for identification of potentially expansive soils (No. FHWA-RD-77-94). United States. Federal Highway Administration. Office of Research and Development.
  43. Madlener R., Kowalski K., Stagl S. 2007. New ways for the integrated appraisal of national energy scenarios: The case of renewable energy use in Austria. *Energy policy*, 35(12), 6060–6074.
  44. González J.A., Ruiz M.D.C. 2006. Bleaching of kaolins and clays by chlorination of iron and titanium. *Applied clay science*, 33(3–4), 219–229.
  45. Hajjaji W., Hachani M., Moussi B., Jeridi K., Medhioub M., López-Galindo A., Jamoussi F. 2010. Mineralogy and plasticity in clay sediments from north-east Tunisia. *Journal of African Earth Sciences*, 57(1–2), 41–46.
  46. Jordan M.M., Montero M.A., Meseguer S., Sanfeliu T. 2008. Influence of firing temperature and mineralogical composition on bending strength and porosity of ceramic tile bodies. *Applied Clay Science*, 42(1–2), 266–271.
  47. Dondi M., Raimondo M., Zanelli C. 2014. Clays and bodies for ceramic tiles: Reappraisal and technological classification. *Applied Clay Science*, 96, 91–109.
  48. Raimondo M., Dondi M., Gardini D., Guarini G., Mazzanti F. 2009. Predicting the initial rate of water absorption in clay bricks. *Construction and Building Materials*, 23(7), 2623–2630.
  49. Milheiro F.A.C., Freire M.N., Silva A.D., Holanda J.N.F. 2005. Densification behaviour of a red firing Brazilian kaolinitic clay. *Ceramics International*, 31(5), 757–763.
  50. Benahsina A., El Haloui Y., Taha Y., Elomari M., Bennouna M.A. 2022. Substitution of natural clay by Moroccan solid mining wastes to manufacture fired bricks. *Materials Today: Proceedings*, 58, 1324–1330.
  51. Dondi M., Guarini G., Ligas P., Palomba M., Raimondo M. 2001. Chemical, mineralogical and ceramic properties of kaolinitic materials from the Tresnuraghes mining district (Western Sardinia, Italy). *Applied Clay Science*, 18(3–4), 145–155.
  52. Hachani M., Hajjaji W., Moussi B., Medhioub M., Rocha F., Labrincha J.A., Jamoussi F. 2012. Production of ceramic bodies from Tunisian Cretaceous clays. *Clay minerals*, 47(1), 59–68.
  53. El Ouahabi M., Daoudi L., De Vleeschouwer F., Bindler R., Fagel N. 2014. Potentiality of clay raw materials from northern Morocco in ceramic industry: Tetouan and Meknes areas. *Journal of Minerals and Materials Characterization and Engineering*, 2, 145.
  54. Dondi M., García T.J., Rambaldi E., Zanelli C., Cabedo V.M. 2021. Resource efficiency versus market trends in the ceramic tile industry: Effect on the supply chain in Italy and Spain. *Resources, Conservation and Recycling*, 168, 105271.